Innovative: International Multi-disciplinary Journal of Applied Technology
(ISSN 2995-486X) VOLUME 02 ISSUE 09, 2024

Using the DFT to Study the Electronic Structure and Optical Properties for Inse Monolayer

Muntazer Abbas Thuwaini Daroui
Karbala University College of Science Department of Physics

Muntazer Mahdi Sahib Daham
University of Kufa, College of Science, Department of Physics

Reem Munther Ahmed Saeed
University of mustansiriyah, College of Science, Department of Physics

Nour Al-Huda Abbas Mohsen Shuwait
University of Kufa Faculty of Science Department of Physics

Abstract:

The geometric and electrical structural computations can now be used to mimic material surfaces thanks to advancements in computer techniques in recent years. The density functional theory is used in all of these computations. The results of our computations indicate that InSe has an indirect energy gap of 1.53 eV. It can be seen that for the pristine case, the majority and minority density of state (DOS) are fully symmetric. According to the phonon calculations, it has been shown from the results that these monolayers are dynamically stable because they have a positive frequency with a frequency value of 231 cm-1 within the Brillouin region. We take into account the optical characteristics up to 35 eV. Our findings demonstrated that it begins in the visible spectrum. Whereas absorption coefficient peaks located in the UV spectrum. The refractive index begins to increase and then decreases with the increase of photon energy and become a constant value of about 0.9 when the photon energy equals 26 eV. As an internal layer coating between the substrate and the UV-absorbing layer, this monolayer high refractive index makes it possible to employ.

1-1 General Introduction

Nanotechnology is an interdisciplinary study which allows us to develop new materials with new, interesting and useful properties. These new materials are nanomaterials made from nanoparticles. Nanoparticles are ultra-small particles with exceptional properties which can direct medicines straight to the place where the human body needs them, they can make materials stronger and they can convert solar energy more efficiently. Nanoparticles possess different properties and behave differently to the classical, larger building blocks of substances. From a scientific point of view, these interesting new properties are not so much the results from the fact that nanoparticles are small, but they result from the fact that a particle consisting of a relatively limited number of molecules behaves and interacts differently with its surroundings for fundamental physical reasons. Nanoparticles and nanomaterials have gained prominence in technological advancements due to their adjustable physicochemical characteristics such as melting point, wettability, electrical and thermal conductivity, catalytic activity, light absorption and scattering resulting in enhanced performance over their bulk counterparts. By controlling the shape, size and internal order of the nanostructures, properties (electrical conductivity, colour, chemical reactivity, elasticity, etc.) can be modified [1,2].

Methodology

2-1 Schrödinger's Equation

Schrödinger equation results from applying the classical wave equation to describe a physical system in which subatomic particles play random motion**,** thereby leading to quantum mechanics. The physical reality described by the wave function is subatomic particle moving randomly. Therefore, the characteristics of quantum mechanics have a dual nature, one of them is the deterministic nature carried over from classical physics, and the other is the probabilistic nature coined by particle's random motion. Based on this model, almost all of open questions in quantum mechanics can be explained consistently, which include the particle-wave duality, the principle of quantum superposition, interference pattern of double-slit experiments, and the boundary between classical world and quantum world. The current quantum mechanics is a mixture of matrix mechanics and wave mechanics, which are sharply conflicting in principle. Matrix mechanics treats quantum particles as classical particles with fixed relation between the particle's position and its momentum. The matrix mechanics, in fact, belongs to the old quantum theory. Both Born's non-commutative relation and Heisenberg uncertainty relation originate from matrix mechanics. However, in wave mechanics, there is no any fixed relation between the particle's position and its momentum, and the particle's position and its momentum belong to immeasurable physical quantities. Therefore, there is no need for non-commutative relation and uncertainty relation in wave mechanics [57].

In the discussion of the particle in an infinite potential well, it was observed that the wave function of a particle of fixed energy E could most naturally be written as a linear combination of wave functions of the form:

$$\psi(x,t) = Ae^{-i(kx-wt)} \quad (2\text{-}1)$$

for a free particle of momentum p = ħ k and energy E = ħw with this in mind, we can then note that:

$$\frac{\partial^2\psi}{\partial x^2} = -k^2\psi \quad (2\text{-}2)$$

Which can be written, using $E = p^2/2m = \frac{-h^2k}{2m}$

$$-\frac{\hbar^2}{2m}\frac{\partial^2 W}{\partial x^2} - \frac{P^2}{2m}\psi \quad (2\text{-}3)$$

Similarly

$$\frac{\partial \Psi}{\partial t} = -i\omega\Psi \quad (2\text{-}4)$$

which can be written, using $E = \hbar\omega$:

$$i\hbar\frac{\partial \Psi}{\partial t} = \hbar\omega\Psi = E\Psi \quad (2\text{-}5)$$

We now generalize this to the situation in which there is both a kinetic energy and a potential energy present, then $E = p^2/2m + V(x)$ so that

$$E\Psi \frac{P^2}{2m}\Psi + (x)\Psi \quad (2\text{-}6)$$

Where " is now the wave function of a particle moving in the presence of a potential V (x). But if we assume that the results Eq. (3) and Eq. (5) still apply in this case then we have

$$-\frac{\hbar^2}{2m}\frac{\partial^2 W}{\partial x^2} + v(x)\Psi = i\hbar\frac{\partial W}{\partial t} \quad (2\text{-}7)$$

2-2 Density functional Theroy (DFT)

Density functional theory (DFT) is one of the most widely used methods for ab initio calculations of the structure of atoms, molecules, crystals, surfaces, and their interactions. Unfortunately, the customary introduction to DFT is often considered too lengthy to be included in various curricula. An alternative introduction to DFT is presented here, drawing on ideas which are well-known from thermodynamics, especially the idea of switching between different independent variables. The central theme of DFT, i.e., the notion that it is possible and beneficial to replace the dependence on the external potential v(r) by a dependence on the density distribution n(r), is presented as a

straightforward generalization of the familiar Legendre transform from the chemical potential μ to the number of particles *N*. This approach is used here to introduce the Hohenberg–Kohn energy functional and to obtain the corresponding theorems, using classical nonuniform fluids as simple examples. The energy functional for electronic systems is considered next, and the Kohn–Sham equations are derived. The exchange- correlation part of this functional is discussed, including both the local density approximation to it, and its formally exact expression in terms of the exchange-correlation hole. A very brief survey of various applications and extensions is included [58-59].

From Schrödinger's equation:

$$i\hbar \frac{\partial}{\partial t}\psi(\vec{r},t) = \hat{H}\Psi(\vec{r},t) \qquad (2\text{-}8)$$

It is often impracticable to use a complete relativistic formulation of the formula; therefore, Schrödinger himself postulated a non-relativistic approximation which is nowadays often used, especially in quantum chemistry. Using the Hamiltonian for a single particle

$$\hat{H} = \hat{T} + \hat{v} = -\frac{\hbar^2}{2m}\vec{\nabla}^2 + \vec{v}(\vec{r},t) \qquad (2\text{-}9)$$

leads to the (non-relativistic) time-dependent single-particle Schrödinger equation

$$i\hbar \frac{\partial}{\partial t}\Psi(\vec{r},t) = [-\frac{\hbar^2}{2m}\vec{\nabla}^2 + v(\vec{r},t)]\psi(\vec{r},t) \qquad (2\text{-}10)$$

In this thesis, from now on only non-relativistic cases are considered. For N particles in three dimensions, the Hamiltonian is.

$$\hat{H} = \sum_{i=1}^{N} \frac{-\hbar^2}{2m_i}\nabla_{(1\,2\,\ldots\,n,)}^2 + V(r\,r\,\cdots r\,.t) = -\frac{1}{2}\sum_{i=1}^{N}\frac{1}{m_i}\nabla_{(1\,2\,\ldots\,n,)}^2 + V(r\,r\,\cdots r\,.t) \qquad (2\text{-}11)$$

2-3 the Generalized Gradient Approximation.

Within density functional theory (DFT), the ground state energy of an interacting system of electrons in an external potential can be written as a functional of the ground state electronic density [80]. When compared to conventional quantum chemistry methods, this approach is particularly appealing since it does not rely on the knowledge of the complete N-electron wave function but only of the electronic density. Unfortunately, although the theory is in principle exact, the energy functional contains an unknown quantity, called the exchange-correlation energy, Exc [ρ], that must be approximated in any practical implementation of the method. Several approximate exchange-correlation functionals have been proposed in the literature, the most commonly used ones being the local density approximation (LDA) and the generalized gradient approximation

(GGA).

The local density approximation [81] is the simplest and most widely used exchange-correlation functional:

$$E[P] = \int P\ (r) \in p(r)\ dr \qquad (2\text{-}16)$$

Always provide sufficiently accurate results. For example, it almost always overestimates the binding energy and underestimates the bond-length of weakly bound molecules and solids [82].

LDA fails also to predict the ground state structure of iron, although the error is quantitatively small [83]. In an attempt to improve upon LDA, a dependence of the exchange-correlation energy on the derivatives of the electronic density can be introduced. A simple and systematic extension of LDA is the gradient expansion approximation (GEA), which is is asymptotically valid for densities that vary slowly over space. For finite systems, the terms in the expansion of the exchange energy of order greater or equal than four diverge while the exchange potential diverges already at second order. By using a constant Bxc determined variationally for each atom, Herman et al. showed that the gradient expansion up to second order yields improved total energies of atoms [84]. An improvement in the exchange energies is also obtained when the exact expansion coefficient for exchange, Bx, is used in an exchange-only calculation [85]. However, the inclusion of correlation in the second order expansion gives energies that are less accurate than LDA [86,87]. The analysis of this failure has lead some authors [88-89] to introduce a generalization of the gradient expansion, whose generic functional [90].

2-4 Hartree-Fock Equation.

The Hartree-Fock approximation, which is equivalent to the molecular Orbital approximation, is central to chemistry. The simple picture, that Chemists carry around In their heads, of electrons occupying orbitals is In Reality an approximation, sometimes a very good one but, nevertheless, an Approximation—the Hartree-Fock approximation. In this chapter we de- Scribe, in detail, Hartree-Fock theory and the principles of ab Initio Hartree- Fock calculations. The length of this chapter testifies to the important role Hartree-Fock theory plays in quantum chemistry. The Hartree-Fock ap- Proximation is important not only for its own sake but as a starting point for more accurate approximations, which include the effects of electron Correlation. A few of the computational methods of quantum chemistry Bypass the Hartree-Fock approximation, but most do not, and all the Methods described in the subsequent chapters of this book use the Hartree- Fock approximation as a starting point. Chapters 1 and 2 introduced the basic concepts and mathematical tools important for an In-depth under- Standing of the structure of many-electron theory. We are now In a position To tackle and understand the formalism and computational procedures asso- Ciated with the Hartree-Fock appreximation, at other than a superficial level. In addition to the basic formalisms of Hartree-Fock theory, this chapter Includes a number of ab initio calculations. These calculations are not In-Cluded as a review of available computational results, but as a means of Illustrating fundamental ideas. The importance of these calculations to an Understanding of the formalisms of this and later chapters cannot be over- Emphasized. To illustrate the Hartree-Fock approximation, we have per-Formed calculations of each of the quantities discussed in the text (total Energies, ionization potentials, equilibrium geometries, dipole moments, ctc,). Using a standard hierarchy of basis sets (STO-3G,4-31G,6-31G and G*) and a standard collection of molecules (H2, CO, N2, CHa,NH331-6- H20 and FH). We thus illustrate the formalism and the accuracy or In The formalisms of those chapters. In this way we can compare calculations From chapter to chapter to see how a perturbation calculation improves the Hartree-Fock dipole moment of CO, to see how a Green's function calcula- Tion improves the Hartree-Fock ionization potentials of N2, etc. The cal-Culations are intimately related to our discussion of the formal methods of Qunatum chemistry. In

addition to these larger calculations, we have used two smaller ab Initio models to Illustrate theory. The minimal basis model of H2, which We introduced in the previous chapter, is applied ubiquitously throughout The book. To specifically illustrate the machinery of Hartree- Fock self-Consistent-field (SCF) calculations. We use the minimal basis model of HeH*This model is perhaps our most important means of describing the SCF Procedure. Appendix A contains a derivation of formulas for all the integrals Required in this HeH* calculation, and Appendix B contains a short FORTRAN program for performing ab initio Hartree-Fock calculations on Any two-electron diatomic molecule using the STO-3G basis set. Included Is the detailed output for the calculation on HeH*+. The,program is written So that it can be easily understood by anyone who has followed the text And has a minimal knowledge of FORTRAN. While it is simple, this program Contains the essential ideas (but not the details) of large, ab initio packages Such as Gaussian 80.1 Appendices A and B and Subsection 3.5.3 are intended To make explicit the basic manipulations of the SCF procedure and take Some of the mystery out of such calculations. In Section 3.1 we present the Hartree-Fock eigenvalue equations and Define and discuss associated quantities such as the coulomb, exchange, and Fock operators. The results of this section are presented without derivation As summary of the main equations of Hartree-Fock theory. Section 3.2 constitutes a derivation of the results of the previous section. The order of presentation of these two sections is such that the derivations Of Section 3.2 can be skipped ifnecessary. For a fuller appreciation of Hartrre-Fock theory

2.6 Fermi Energy

The Fermi energy is a fundamental property of an electron system, and thermodynamic measurements which probe the Fermi energy or density of states are key to understanding the host material band structure and elec- tron interaction effects. Although a number of thermo- dynamic properties, such as specific heat [109, 110] magne- tization [111], magnetocapacitance [112], or compressibility [113] can probe the density of states in an electron system, accessing them experimentally becomes increasingly diffi- cult at the micro- and nano-scale. In the case of grapheme [114], magnetization and specific heat measurements are ex- ceedingly difficult, and the accuracy of compressibility [115] and capacitance measurements [116–117] are also limited by the reduced sample dimensions. Using a graphene dou- ble layer heterostructure, we describe a technique which allows a direct measurement of the Fermi energy in an electron system with an accuracy which is independent of the sample size. The underlying principle of the method discussed here is that an interlayer bias applied to bring the top layer to the charge neutrality point is equal to the Fermi energy of the bottom layer. We illustrate this technique by probing the Fermi energy in monolayer graphene, both at zero and in high magnetic fields. We show that this method allows an accurate determination of the Fermi velocity, Landau level spacing, and Landau level broadening in monolayer grapheme. Our samples are independently contacted grapheme double layers, consisting of two graphene single layers separated by a thin dielectric [118]. To fabricate such devices, we first mechanically exfoliate the bottom graphene layer from natural graphite onto a 280 nm thick SiO2 dielectric, thermally grown on a highly doped Si substrate. Standard e-beam lithography, Cr/Au deposition followed by lift-off, and O2 plasma etching are used to define a Hall bar device. A 4 to 7 nm top Al2O3 dielectric layer is deposited on the bottom layer by atomic layer deposition (ALD), and using evaporated Al as a nucleation layer. The dielectric film thickness grown on graphene is further verified by transmission electron microscopy in multiple samples. To fabricate the graphene top layer, a separate graphene single layer is mechanically exfoliated on a SiO2/Si substrate. After spin-coating polymetyl metacrylate (PMMA) on the top layer and curing, we etch the underlying substrate with NaOH, and detach the top layer along with the align- ment markers captured in the PMMA membrane. The membrane is transferred onto the bottom layer device, and aligned. A Hall bar is subsequently defined on the top layer, completing the double layer graphene device. Three

samples were investigated in this study, all with similar results. We focus here on data collected from one sample with a 7.5 nm thick interlayer dielectric, and with an interlayer resistance larger than 1 G. Both layer mobilities are 10,000 cm2/V·s. Using small signal, low frequency lock-in techniques we probe the layer resistivities as a function of back-gate bias (VBG), and the inter-layer bias (VTL) applied on the top layer. The bottom layer is maintained grounded during measurements. data show the longitudinal resistivity of the bottom (B) and top (T) layer measured as a function of VTL, and at different VBG values [119]. The data B,T vs. VTL exhibit the ambipolar behavior characteristic of graphene, and with a charge neutrality point which is VBG-dependent. The shift of the charge neutrality point of the bottom layer as a function of VBG is explained by picturing the bottom layer as a dual-gated graphene single layer, with the Si substrate as back-gate and the top graphene layer serving as top-gate. The dependence of the T vs. VTL data on VBG is more subtle, and implies an incomplete screening by the bottom layer of the back-gate induced electric field.

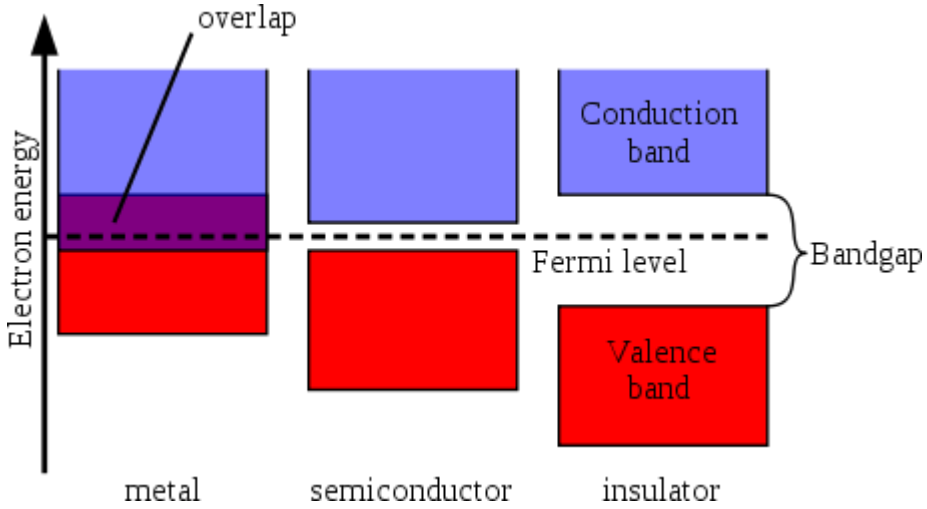

Figure (1-2): Comparison of Fermi energy between conductive materials, semiconductors, and insulators.

2-7 Computation Detail

We used an efficient computer code to perform ab initio calculations, known as CASTEP [125], which is based on the standard Kohn–Sham self- consistent density functional theory (DFT). Using density functional theory (DFT), this is implemented in the Cambridge Serial Total Energy Package (CASTEP) program, within the projected augmented wave (PAW) procedure, and is used for all computations in this work [126]. The exchange-correction function is given using the generalized gradient approximation (GGA) put out by Perdew, Burke, and Ernzerhof (PBE). CASTEP can be considered the first mechanical program used to implement the electronic structure of computations. The functional density of crystalline solids, surfaces, molecules, fluids, and amorphous materials; can be used to simulate these materials. To calculate the characteristics of the materials used in the study can be considered as a set of nuclei and electrons. The most important requirements for computers used are high speed and memory [127]. For example, we can calculate several properties for monolayer in this thesis such as structural properties (bond length and angles), electronic properties (density of state and band structure), optical properties (conductivity, absorption, reflectivity, refractive index, loss function, and dielectric function) and phonon dispersion.

The complex dielectric function is formed by summation the real and imaginary parts as follow:

$$\varepsilon(\omega) = \varepsilon_1(\omega) + i\varepsilon_2(\omega) \qquad (2-21)$$

Where the real part $\varepsilon_1(\omega)$ and imaginary part $\varepsilon_2(\omega)$are given by the well-known relations

$$\varepsilon_1(\omega) = 1 + \frac{2}{\pi} P \int_0^{\infty} \frac{\omega' \varepsilon_2(\omega')}{\omega'^2 - \omega^2} d\omega' \qquad (2-22)$$

$$\varepsilon_2(\omega) = \frac{e^2\hbar}{\pi m^2 \omega^2} \sum_{v,c} \int_{BZ} |\langle u_{cv}|u.\nabla|u_{ck}\rangle|^2 \, \delta[\omega_{cv}(k) - \omega] \, d^3k \quad (2-23)$$

Results and Discussion

3.1 Structural and Electronic Properties

Our available computations show that the optimal structure for the InSe monolayer is shown in Figure (1.4) with a thickness of 5.349Å. InSe monolayer, the lattice constant is 4.050Å. Furthermore, our computations demonstrated that the estimated bond lengths of 2.517Å between the In and Se in the InSe monolayer atom are compatible. The InSe monolayer's indirect energy gaps are 1.53 eV. As seen in Figure (1.5), the indirect energy gap was found to be between the valence Γ point and the conduction M point. Using first-principles calculations, the indirect energy gap of the InSe monolayer has previously been verified.

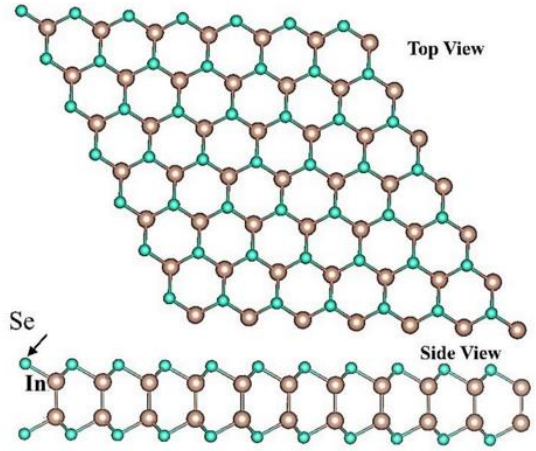

Figure (1.4): The geometric structure of top and side of the InSe monolayer.

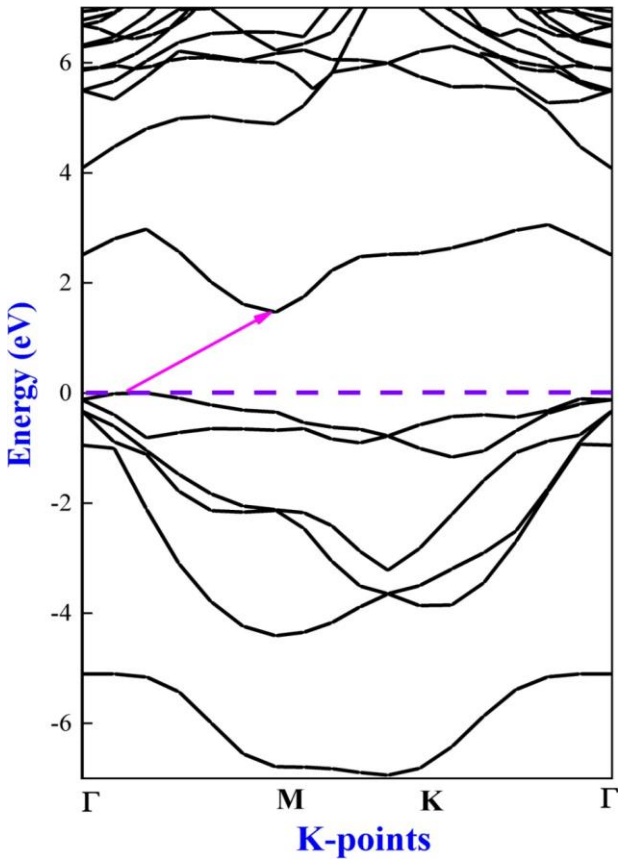

Figure (1.5): The calculated band structure of InSe monolayer. The dashed line represent the Fermi level.

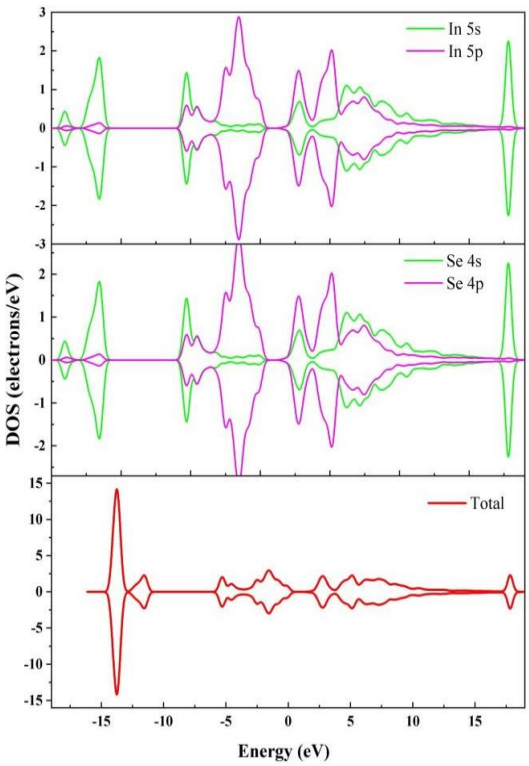

Figure (1.6): The total and partial density of state of InSe monolayer.

The partial DOS and total density of states (TDOS) of this system are shown in Figure (1.6). Observing that the majority and minority DOS are exactly the same in fundamental states suggests that both will be replaced by states that are not electronic for a two-dimensional InSe monolayer. Figure (1.6) shows that the electrons of the In atom have a bigger contribution for the p- orbit and a lower contribution for the s-orbit, whereas the electrons of the Se atom have a larger contribution and a lower contribution. This relates to the partial density of state's valence band, which is close to the Fermi level.

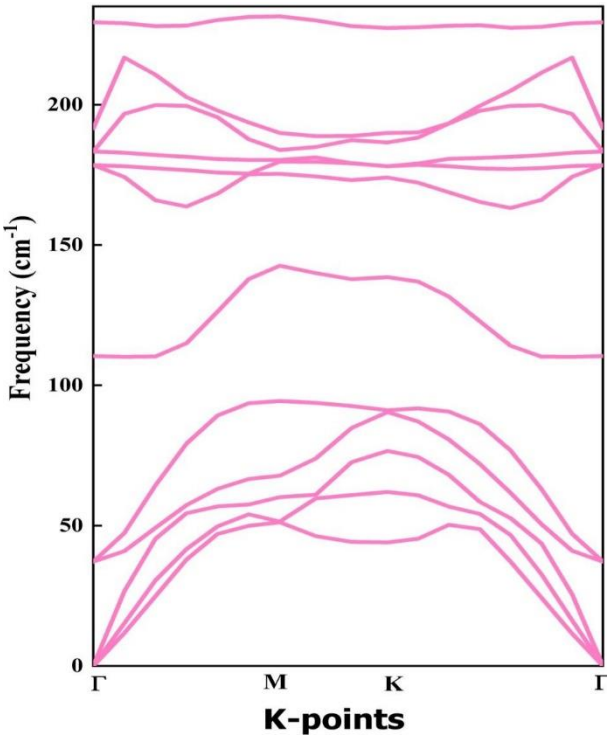

Figure (1.7): Phonon dispersion curve of InSe monolayer.

Figure (1.7) explains the phonon dispersion curve for the InSe monolayer. Observe the positive-frequency phonon type present in the Brillouin zone. The system's dynamic balance is thus demonstrated by this outcome. The frequency value for the InSe monolayer is also shown to be 231 cm^{-1}.

3.2 Optical properties

The calculations of optical properties of InSe monolayer are implemented in the energy range 0-35 eV employing the normal incident polarization light. The study of optical properties is extremely necessary for their possible application in different fields. The real and imaginary part of dielectric function as a function of the incident photon energy for both monolayer is plotted in Figure (1.8) (a). The maximum peak of real part for InSe is 5.02 at energy 3.03 eV, these points out the storage energy (high polarization). When the photon energy increases, the real part rapidly decreases, and it becomes constant at approximately 20 eV. Meanwhile, when the real part decreases, the imaginary part increases and the maximum peak of InSe monolayer is 4.80 occur at 4.06 eV. The imaginary part represented the absorption coefficient of the medium. Thus, this monolayer can be used in photovoltaic devices especially in the ultraviolet region. The higher refractive index for InSe monolayer, can be utilized in several applications, for instance, manufacturing optoelectronic devices. It can be noticed from Figure (1.8) (b), the refractive index begins to increase and then decreases with the increase of photon energy and become a constant value of about 0.9 when the

photon energy equals 26 eV for InSe monolayer. Also notice that maximum values are 2.32 at 3.22 eV.

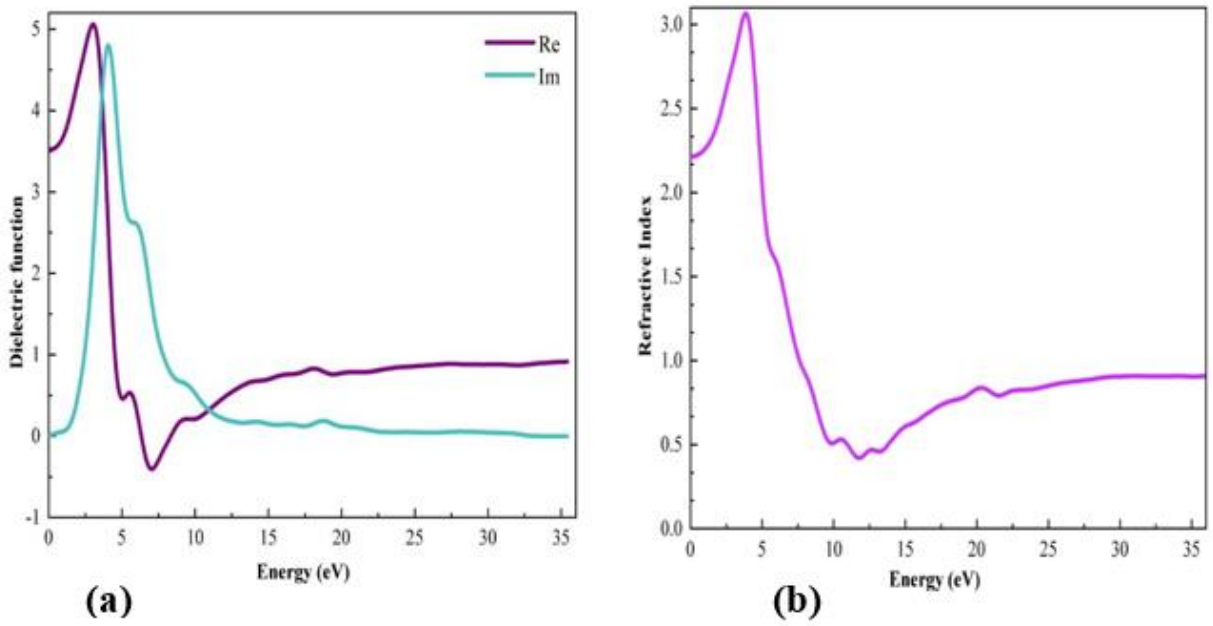

Figure (1.8) :(a) the real and the imaginary part of dielectric function and (b) the refractive index InSe monolayer.

Figure (1.9) (c), shows the reflectivity as a function of photon energy. The maximum values of the computed reflectivity are respectively about 25.5% for InSe monolayer, occurs in UV region at energy 7.12 eV. The absorption coefficient for InSe monolayer is illustrated in Figure (1.9)(d), the absorption coefficient associated with the imaginary part of the dielectric function. The maximum peak of absorption spectra is 11.9 × 104cm−1 observed at about 7 eV. After 8 eV, the absorption coefficient decreases rapidly with the photon energy. That is means that monolayer have greater potential in application of photoelectronic devices.

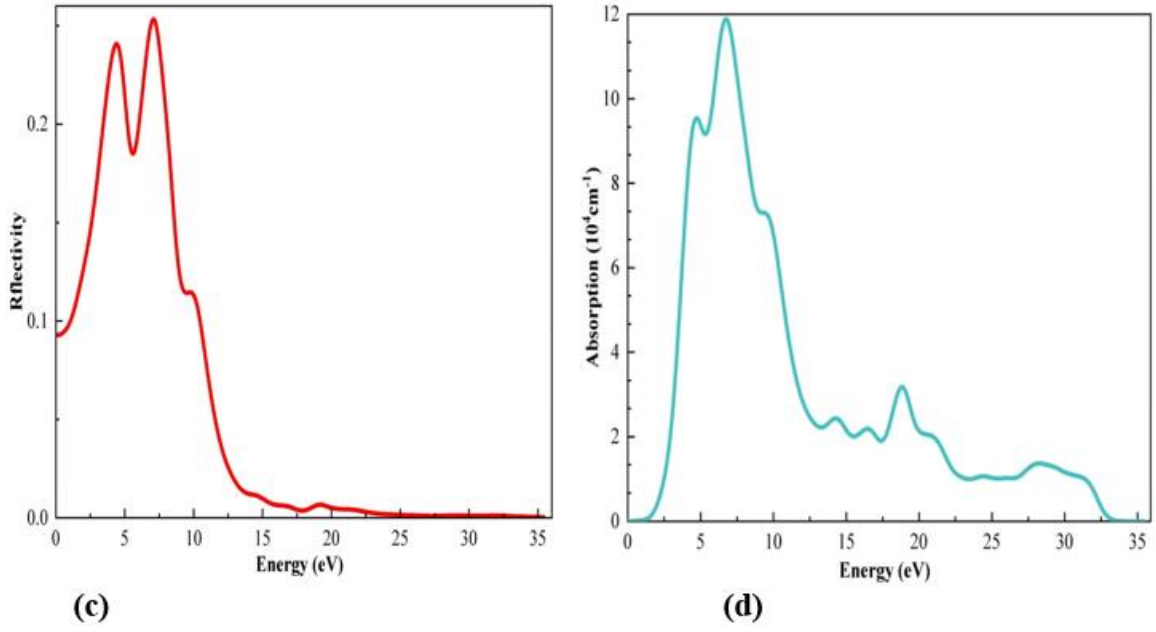

Figure (1.9): (c) the optical reflectivity and (d) absorption coefficient of InSe monolayer.

we observed that the conductivity of monolayer is located at the UV region. This means the possibility of using these materials as used ultraviolet detectors. Finally, the computed loss function is depicted in Figure (1.10) (f). The loss function represented the mixed plasma frequency and optical properties. The material acts as metallic nature below the plasma frequency and beyond it demonstrates the dielectric nature. The maximum value of loss function is 1.78 observed at 11.20 eV for InSe. According to this result, the monolayer can be employed in the solar cell applications.

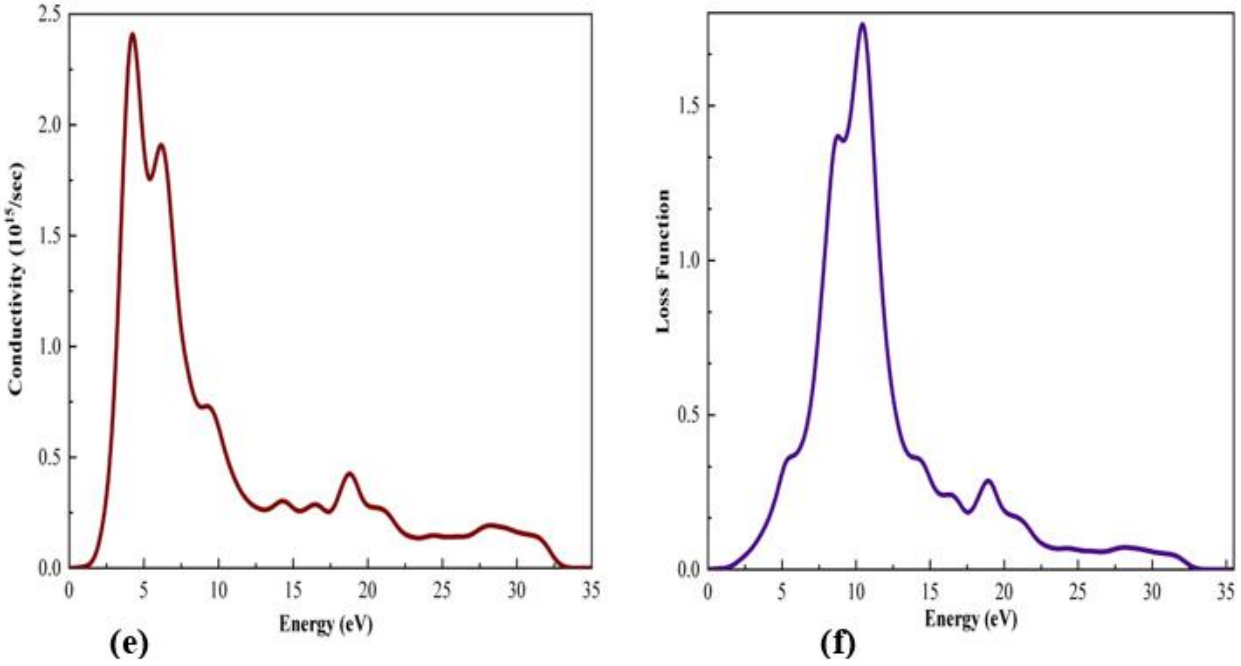

Figure (1.0): (e) the optical conductivity and (f) Loss function of InSe monolayer.

References

1. Y. Shao, H.P. Zhao, X.Q. Feng, Optimal characteristic nanosizes of mineral bridges in mollusk nacre, RSC Adv. 4 (61) (2014) 32451-32456.
2. S. Keten, M.J. Buehler, Atomistic model of the spider silk nanostructure, Appl. Phys. Lett. 96 (15) (2010) 153701.
3. Gao, P.; Xiao, Y.; Li, L.; Li,W.; Tao,W. Biomedical applications of 2D monoelemental materials formed by group va and via:A concise review. J. Nanobiotechnol. 2021, 19, 1–23. [CrossRef] [PubMed]
4. Mei, X.; Hu, T.; Wang, Y.; Weng, X.; Liang, R.; Wei, M. Recent advancements in two-dimensional nanomaterials for drug delivery. Wiley Interdiscip. Rev. Nanomed. Nanobiotechnol. 2020, 12, e1596. [CrossRef] [PubMed]
5. Rao, C.E.E.; Sood, A.E.; Subrahmanyam, K.E.; Govindaraj, A. Graphene: The new two-dimensional nanomaterial. Angew. Chem. Int. Ed. 2009, 48, 7752–7777. [CrossRef]
6. Novoselov, K.S.; Geim, A.K.; Morozov, S.V.; Jiang, D.E.; Zhang, Y.; Dubonos, S.V.; Grigorieva, I.V.; Firsov, A.A. Electric field effect in atomically thin carbon films. Science 2004, 306, 666–669. [CrossRef]
7. Geim, A.K.; Novoselov, K.S. The rise of graphene. In Nanoscience and Technology: A Collection of Reviews from Nature Journals;World Scientific: Singapore, 2010; pp. 11–19.

8. Chung, C.; Kim, Y.-K.; Shin, D.; Ryoo, S.-R.; Hong, B.H.; Min, D.-H. Biomedical applications of graphene and graphene oxide. Acc. Chem. Res. 2013, 46, 2211–2224. [CrossRef] [PubMed]
9. Tawfik A. Saleh, "Nanomaterials: Classification, Properties, and Environmental toxicities", Journal “Environmental Technology & Innovation", 20 (2020) 101067.
10. H. W. Kroto, J. R. Heath, S. C. O'Brien, R. F. Curl, and R. E. Smalley. C60 buckminsterfullerene. Nature, 318:162{163, 1985.
11. Freitas RA., Jr Nanodentistry. J Am Dent Assoc. 2000; 131:1559–65.
12. Gao Li, Rongchao Jin, and Catalysis by gold nanoparticles: carbon-carbon coupling reactions, Nanotechnol Rev 2013; 2(5): 529–545.
13. Santosh Bahadur Singh, Praveen Kumar Tandon, Catalysis: A Brief Review on Nano-Catalyst, Journal of Energy and Chemical Engineering, 2014, 2, 3, pg.106-115.
14. W.-W. Tang, G.-M. Zeng, J.-L. Gong et al., ―Impact of humic/fulvic acid on the removal of heavy metals fromaqueous solutions using nanomaterials: a review,‖ Science of the Total Environment, vol. 468-469, pp. 1014–1027, 2014.
15. Yan J., L. Han,W. Gao, S. Xue, andM.Chen, ―Biochar supported nanoscale zerovalent iron composite used as persulfate activator for removing trichloroethylene,‖ Bioresource Technology, vol. 175, pp. 269– 274, 2015.
16. Liu F., Yang J. H., Zuo J. et al., ―Graphene-supported nanoscale zero- valent iron: removal of phosphorus from aqueous solution and mechanistic study,‖ Journal of Environmental Sciences, vol. 26, no. 8, pp. 1751–1762, 2014.
17. Kalhapure R. S., Sonawane S. J., Sikwal D. R. et al., ―Solid lipid nanoparticles of clotrimazole silver complex: an efficient nano antibacterial against Staphylococcus aureus and MRSA, Colloids and Surfaces B: Biointerfaces, vol. 136, pp. 651–658, 2015.
18. Haijiao Lu, Jingkang Wang, Marco Stoller, Ting Wang, Ying Bao, Hongxun Hao, An Overview of Nanomaterials for Water and Wastewater Treatment, Advances in Materials Science and Engineering, Volume 2016, Article ID 4964828, http://dx.doi.org/10.1155/2016/4964828
19. Zhao, Z.M.; Sun, J.; Xing, S.M.; Liu, D.J.; Zhang, G.J.; Bai, L.J.; Jiang, B.L. Enhanced Raman scattering and photocatalytic activity of TiO2 films with embedded Ag nanoparticles deposited by magnetron sputtering. J. Alloys Compd. 2016, 679, 88–93.
20. Guo, Q.; Zhou, C.Y.; Ma, Z.B.; Ren, Z.F.; Fan, H.J.; Yang, X.M. Elementary photocatalytic chemistry on TiO2 surfaces. Chem. Soc. Rev. 2016, 45, 3701–3730.